Check for updates

Received: 1 July 2022 | Revised: 28 September 2022 | Accepted: 22 October 2022

DOI: 10.1002/pen.26186

RESEARCH ARTICLE

POLYMER ENGINEERING AND SCIENCE WILEY

Development of a low-cost volumetric additive manufacturing printer using less viscous commercial resins

Ribin Varghese Pazhamannil[1] | **Haitham M. Hadidi**[2] | **Govindan Puthumana**[1]

[1]Department of Mechanical Engineering, Government College of Engineering Kannur, APJ Abdul Kalam Technological University, Thiruvananthapuram, India

[2]Department of Mechanical Engineering, College of Engineering, Jazan University, Jazan, Kingdom of Saudi Arabia

Correspondence
Ribin Varghese Pazhamannil, Department of Mechanical Engineering, Government College of Engineering Kannur, APJ Abdul Kalam Technological University, Thiruvananthapuram, Kerala, India.
Email: ribinvarghese18@gmail.com

Funding information
TEQIP Four Funds GCE Kannur

Abstract

The technological development of the 3D printing industry has been tremendous starting from stereolithography in the 1980 s. Low throughput and surface quality had been the major obstacles to this technology, which offers very limited constraints to the geometrical shapes. In this work, we designed a low-cost volumetric 3D printer that, unlike traditional 3D printers, polymerizes the whole geometry within the revolving resin container. Optimized projections needed for the polymerization of target objects were developed in MATLAB R2020b using the concepts of tomographic reconstruction. The rotation of the resin container and the projections rate were matched to develop the target geometries after the oxygen depletion. Commercially available low viscous Anycubic plant-based resins were used as the printing material. 3D objects of centimeter scale could be manufactured in 30 seconds with extremely low surface roughness in the sub-micron range. The dimensional deviation of final components from the CAD model was found to be within 5%. The over-printing on existing solid structures was successfully experimented with and thus opens the way for future developments. Commercialization of volumetric 3D printers would result in mass production of complex customer-specific functional components which in turn boosts the manufacturing sector significantly.

KEYWORDS

3D printing, photopolymerization, tomography, volumetric additive manufacturing

1 | INTRODUCTION

The popularity of additive manufacturing technologies is attaining more reach due to their capability to fabricate complex customer-specific components. Ever since its inception in the 1980 s with the process of stereolithography, 3D printing has transformed the production sector.[1–3] There has been a substantial shift in the production paradigm resulting in parts and geometries that were previously unattainable through traditional approaches becoming increasingly popular. Existing AM technologies use point-at-a-time (0D), line-at-a-time (1D), or layer-at-a-time (2D) printing cycles to finish items for end-user advantages.[4–7] Processes such as fused filament fabrication (FFF), stereolithography (SLA), and selective laser sintering (SLS) are examples of point-at-a-time printing. It repeats the printing of each point to get the defined target shape. Line-at-a-time printing includes a material or binder jetting procedure in which a group of nozzles is utilized to print the complete line-at-once.

 © 2022 Society of Plastics Engineers.

15482634, 0, Downloaded from https://onlinelibrary.wiley.com/doi/10.1002/pen.26186 by Egyptian National Sci. Network (Enstinet), Wiley Online Library on [09/11/2022]. See the Terms and Conditions (https://onlinelibrary.wiley.com/terms-and-conditions) on Wiley Online Library for rules of use; OA articles are governed by the applicable Creative Commons License

Projection stereolithography is an example of layer-at-a-time printing. These approaches reduce productivity, decrease surface quality, lengthen post-processing duration, restrict geometric flexibility, or might create mechanical properties anisotropy.[8] Dual-wavelength photopolymerization method,[9] continuous liquid interface production (CLIP),[10] xolography,[11] etc., were the recent advances in the 3D printing industry to enhance print speed and surface properties of customized components. Photopolymer resins containing initiators and inhibitors with two-wavelength projections led to polymerization blockage resulting in liquid resin of designed width for the continuous lifting of cured parts in the dual-wavelength method. CLIP technology employed oxygen permeable membranes to inhibit photopolymerization just above the glass window for the faster continuous lifting of parts from the pool of resin.[12] The dead zone width generated was the key to the success of this process and is formulated as:

$$\text{Dead zone width} = k\left[\frac{\Phi\alpha_{PI}}{D_C}\right]^{-0.5} \quad (1)$$

where, k is the proportionality constant, Φ is the photon intensity, α_{PI} is the absorption coefficient, and D_C is the photopolymer curing dose.

Separation stresses generated during the elevation of the build plate were reduced significantly in these methods. Micro-needles production,[13] sports shoes,[14] etc., were a few applications of CLIP explained in the literature. Xolography is a two-color technology that employs photo switchable initiators to trigger regional polymerization within a constrained monomer volume after linear stimulation with overlapping light rays of distinct wavelengths.

Shusteff et al. invented volumetric additive manufacturing (VAM) in 2017,[15] which is capable of polymerizing the entire target item within the resin vessel. With the superimposition of three orthogonal light rays, volumetric printing was accomplished. The biggest barrier to commercialization was the technology's use of multiple optical instruments. The volumetric creation of complicated geometries utilizing computed tomography ideas was effectively shown in.[16] By beaming light rays in the form of 2D projections onto the pre-controlled revolving resin volume, all of the appropriate points inside the target shape were polymerized simultaneously. The total dosage received was sufficient to generate the target objects. Even though computed tomography 3D printing can build complicated products with better throughput and a larger choice of printer-friendly materials, its accuracy is restricted to 300 μm. Loterie et al.[17] illustrated how a low etendue setup creates significant features and an embedded feedback signal can be used to precisely regulate the polymerization dynamics over the full build region and increase the geometric accuracy of the product solidification. The use of regularly used acrylate resins was altered in[18,19] to demonstrate the use of thiol-ene resins. The shape memory effect could be easily achieved using these resins. Mechanical qualities might be easily altered by varying the amounts of isocyanurate and triethylene glycol. Components in microscale were developed using the computed axial lithography method with silica-mixed photopolymer resin. Optical components fabrication using silica glass is demonstrated in.[20] The green parts developed were sintered to get the smooth glass objects having a Ra value of 6 nm.[21] Sophisticated large strength structures and lattice objects with the smallest features of about 50 μm were printed using the volumetric approach. The VAM approach is used to fabricate complex ceramic components in preceramic polymer resins. In the post-processing method, pyrolysis converts the green parts produced after illumination from multiple angles into ceramics in an oven. Elimination of support structures and capability of overhangs production increases its merits.[22] An improved optimization technique to fabricate exact target geometries using quasi-Newton L-BFGS-B was presented in.[23] Jorge et al.[24] studied the importance of light scattering in photo resins. It entails describing how the photosensitive resin distorts light and computational adjustment to the light patterns to offset the impact of scattering. The experimentation of VAM in the solid-state and shape memory application defining the water capacity is explained in.[25] Another approach lays the road to next-level 3D printing with real-time fault identification and rectification by including form measurement in the manufacturing process. The inclusion of 3D metrology in VAM has helped in the improvement of the accuracy of final models with high scattering in liquid photo resins.[26] Single-photon VAM of ceramic materials was demonstrated in.[27] The preparation of high viscous resins for each VAM trial is tedious and the usage of a commercially available resin would achieve faster enhancement in the technology and thus lead to commercialization.

In this study, we develop a novel design for the volumetric 3D printer which fabricates target geometries using less viscous resins in rotating containers. The demonstration of VAM in commercial resins instead of highly viscous acrylates or hydrogels has not been reported so far. Centimeter range samples were manufactured in a very quick span of 30 seconds. The entire system is based on the principle of computed tomography employed in the medical sector.

15482634, 0, Downloaded from https://onlinelibrary.wiley.com/doi/10.1002/pen.26186 by Egyptian National Sci. Network (Enstinet), Wiley Online Library on [09/11/2022]. See the Terms and Conditions (https://onlinelibrary.wiley.com/terms-and-conditions) on Wiley Online Library for rules of use; OA articles are governed by the applicable Creative Commons License

2 | MATERIALS AND METHODS

The target geometries are initially designed in CAD software before being translated to stl file formats, similar to other commercial 3D printers. The target model is partitioned into pre-set voxels. The tomographic reconstruction principle is used to create the projections necessary for volumetric printing. Radon transform and the Fourier Slice Theorem help in generating initial projections needed for volumetric printing. Iterative optimization after thresholding generates optimized projections required at corresponding angles based on the rotation rate of the resin holder. The superimposition of all light beams produces the necessary level of energy dosage required for the curing of photopolymer resin. The threshold intensity level is required for photopolymerization inhibition in non-target areas. The working principle for volumetric 3D printing is described in Figure 1. The whole computation was performed in MATLAB R2020b to generate the optimized projections set required for volumetric printing.

BenQ MS 610 DLP projector was used for projecting the images of target 3D objects at the respective angles. The SVGA resolution system had 4000 ANSI lumens and a 20,000:1 contrast ratio. A focusing lens of 5 cm focal length was used for projecting images onto the rotating Borosil container. DC gear motor of 3.5 rpm 12 V was used for rotating the container in an exact match with the projection images. The position adjuster helped in adjusting the container position for focus perfection. A labeled CAD model of the experimental setup is shown in Figure 2. Post-curing unit with a UV torch having 40 W 405 nm light intensity is used for curing the parts manufactured from the printer.

Anycubic Eco UV resin was utilized as the photopolymer material to create environmentally safe and bio-

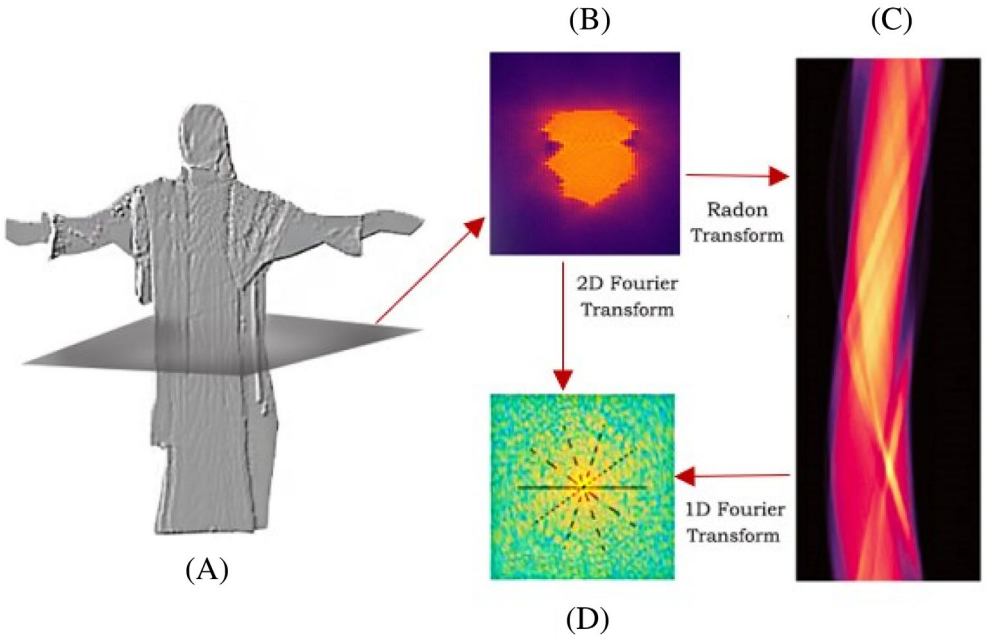

FIGURE 1 (A) Christ the redeemer statue, (B) z-slice, (C) radon transform, and (D) 2D Fourier transform

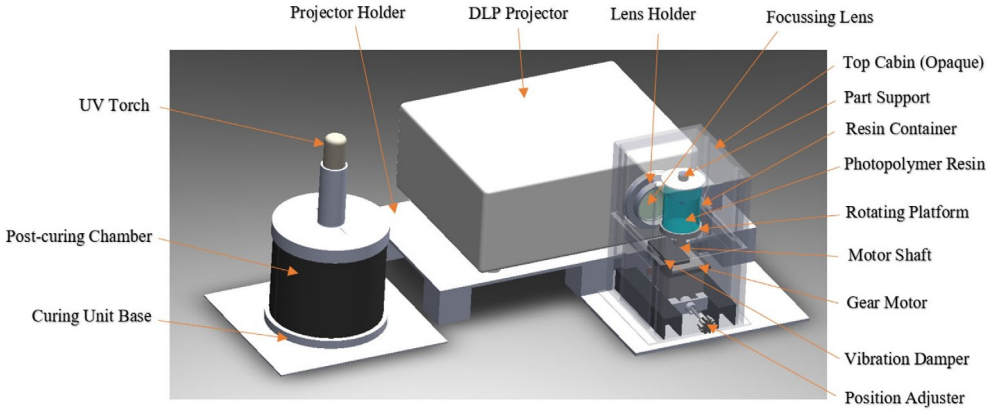

FIGURE 2 Labeled CAD model of the volumetric 3D printer

15482634, 0, Downloaded from https://onlinelibrary.wiley.com/doi/10.1002/pen.26186 by Egyptian National Sci. Network (Enstinet), Wiley Online Library on [09/11/2022]. See the Terms and Conditions (https://onlinelibrary.wiley.com/terms-and-conditions) on Wiley Online Library for rules of use; OA articles are governed by the applicable Creative Commons License

TABLE 1 Resin properties

Resin parameters	Values
Hardness	89D
Viscosity (25°C)	150–350 cP
Shrinkage	1.88%–2.45%
Solid density	1.05–1.25 g/cm^3
Elongation at break	8%–12%
Thermal deformation	80°C
Bending strength	59–70 MPa

degradable 3D objects. Clear resins derived from soybean oil exhibited a very low odor and shrinkage. Table 1 displays the resin characteristics. The plant-based resin demonstrated high resilience and hardness. The resin contains 45% epoxidized soybean oil, making it a more ecologically friendly substance than conventional 3D printing resins. The photopolymer was acceptable for the majority of LCD/DLP 3D printers. Commercially available 3D printing resins can be used as the printing material in contrast to the high viscous resins employed in the volumetric 3D printer developed by Kelly et al.[28] Characterization techniques such as UV–Visible spectroscopy, Fourier Transform Infrared Spectroscopy (FTIR) spectroscopy, and Differential Scanning Calorimetry (DSC) were used to study the resin properties in detail. Lasany LI-2700 UV–Visible spectrophotometer was used to get the absorption spectra. The equipment had a wavelength scan range of 190 nm to 1100 nm. The double beam system had two cuvette holders and a bandwidth of 1 nm. NETZSCH DSC 204-F1 Phoenix was used to study the thermal properties of the plant-based resin. The equipment had an operating temperature between −100°C and 200°C. A gas-tight measurement unit is used, and the exhaust gas is controlled by a mass flow controller. The crucible is made of aluminum and has a maximum power of 9.9 W/cm^2. Nicolet iS50 FTIR spectrometer was used to determine the functional groups and bonding before and after the curing process of Anycubic Eco UV resin.

3 | RESULTS AND DISCUSSION

The computation algorithm for the selected model 'Christ the Redeemer' was performed in MATLAB R2020b. The stl model converted from CAD was voxelized and the existence of the material of the target 3D object is represented by '1'. Radon transform performed on every z-slice of the target for 360° rotations generated the initial set of values for imaging.

$$R\varphi(u,\psi) = \int \varphi(v\sin\psi + u\cos\psi, -v\cos\psi + u\sin\psi)dv \quad (2)$$

where, ψ represents the projection angle, v represents the arc length, and u represents the distance of each line from the origin.

The inverse Radon transform theoretically matched the 3D geometry to be printed. The negative projections created after filtering stood as a hindrance and thus Otsu thresholding followed by gradient descent iterative approach generated final projections to be delivered. The final optimum projections set are displayed in Figure 3 and dose representations at respective heights are shown in Figure 4. The region beyond the boundary of the dose slices represents dark voxels thereby no photopolymerization occurs. The material's non-linear behavior attributed to oxygen interference is critical for determining the dosage limit for the curing process. The curing process is controllable and projections must be shut down after the successful volumetric curing reactions to avoid any undesirable curing. With the reduction in angular spacing for projections, the iterations required to obtain the minimal error between the target and acquired geometry were found to be decreasing. Proper output projections were obtained when radon transform was applied for over 360 sets of angles.

The volumetric 3D printer developed so far can print customized 3D samples within high viscous photo resins. The viscosity is needed to hold the cured part inside the liquid. Thus, highly viscous resins need to be formulated before the fabrication of the setup. A viscosity of at least 4000 cP is necessary to prevent the cured component from sinking. Hydrogels having viscosity near 100,000 cP were successfully printed using the Computed Axial Lithography setup developed by Kelly et al. In this study, we develop a novel design for the volumetric 3D printer which can be used with commercial photo resins used in the stereolithography 3D printing process. The viscosity of the photopolymer resins is in the range of 150–700 cP. Figure 5 depicts the fabricated printer. Light is supplied from the BenQ DLP projector having SVGA resolution in the form of two-dimensional images of the target object to produce the necessary curing dosage required for the photopolymerization initiation. Thereby, volumetric polymerization takes place within the rotating Borosil container in contrast to serial repetition processes as in conventional 3D printers. The resin container shown in the figure has a capacity of 50 ml. The rotation rate of the platform and the angular projections are matched to perfection for precise volumetric printing. Support is provided from the top of the container using very thin

15482634, 0, Downloaded from https://onlinelibrary.wiley.com/doi/10.1002/pen.26186 by Egyptian National Sci. Network (Enstinet), Wiley Online Library on [09/11/2022]. See the Terms and Conditions (https://onlinelibrary.wiley.com/terms-and-conditions) on Wiley Online Library for rules of use; OA articles are governed by the applicable Creative Commons License

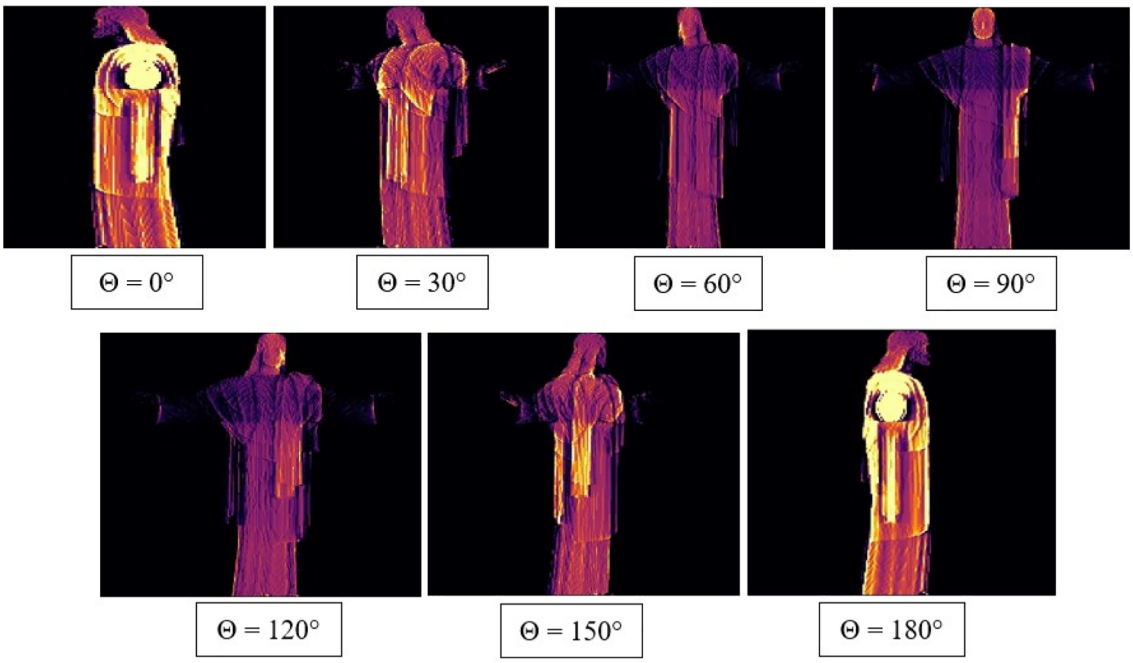

FIGURE 3 Final projections of Christ the redeemer at corresponding angles

FIGURE 4 Dose slices at the corresponding heights of Christ the redeemer

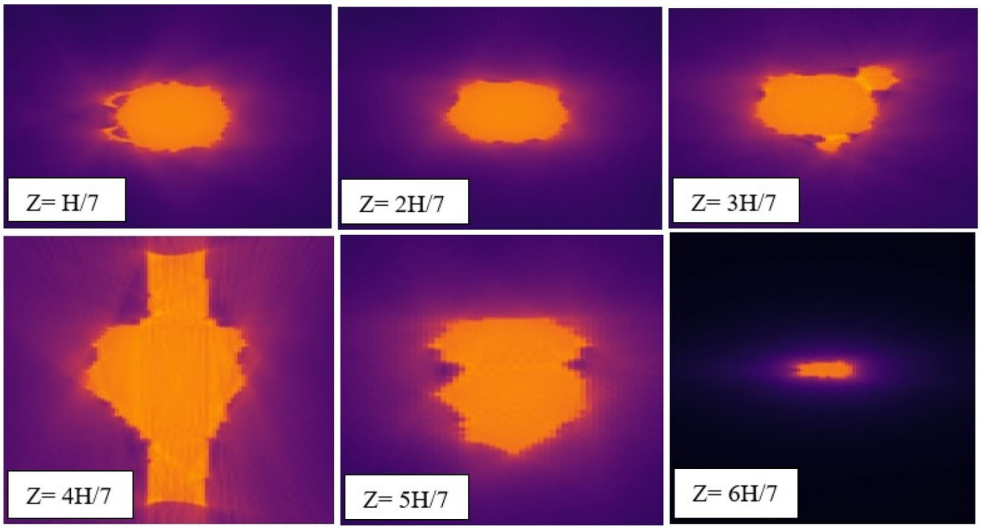

height-adjustable needles. This will help in preventing the part formed from any rotational movement inside the container. The main advantage of the design is to volumetrically fabricate customized components within commercially available low viscous resins. The need for support for 3D printed components has started from the beginning of this technology. The usage of the thin needle can be employed to prevent the part from sinking by holding it from the top. The height of the needle can be varied based on the size and shape of the target object. Small support is only needed to hold the component in its position due to the simultaneous photopolymerization of the target areas. The cumulative energy dosage and the single support successfully produce required 3D objects. The requirement of high viscous resins to hold the cured part is thus eliminated. The light intensity should also be adjusted to avoid any unwanted curing in non-target regions. The parts printed are washed in isopropyl alcohol and post-cured in the post-curing UV chamber having 40 W intensity. The UV torch with 405 nm wavelength helped in the post-curing of the green parts fabricated. The inside area of the curing box was fixed with reflectors for maximum efficiency of the system. The curing box, electronics holder, cabins, lens holder, position adjuster, supports, and platforms were developed using

15482634, 0, Downloaded from https://onlinelibrary.wiley.com/doi/10.1002/pen.26186 by Egyptian National Sci. Network (Enstinet), Wiley Online Library on [09/11/2022]. See the Terms and Conditions (https://onlinelibrary.wiley.com/terms-and-conditions) on Wiley Online Library for rules of use; OA articles are governed by the applicable Creative Commons License

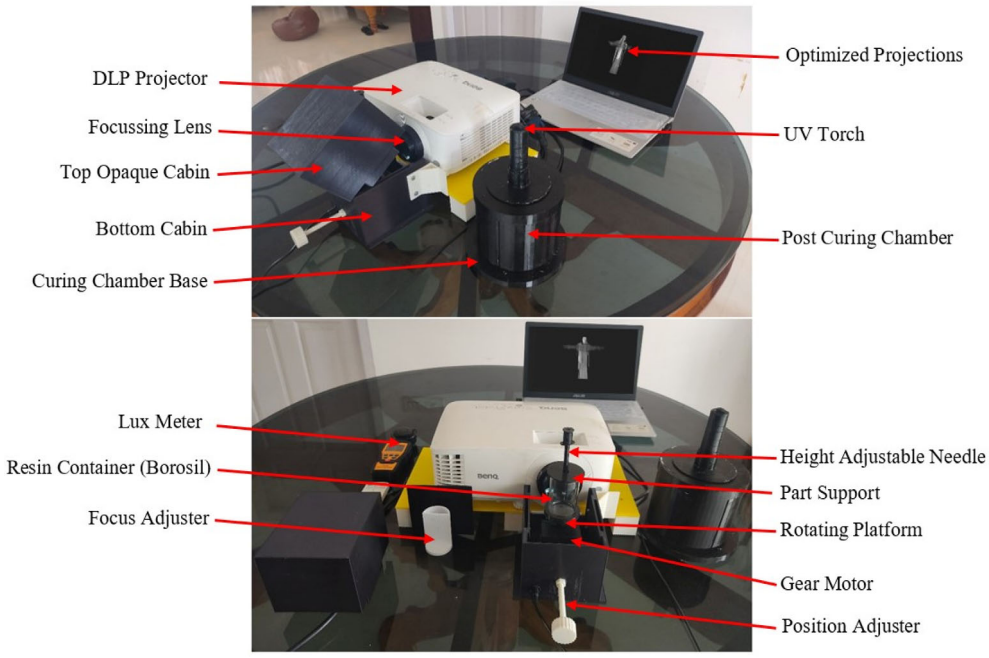

FIGURE 5 Fabricated volumetric 3D printer

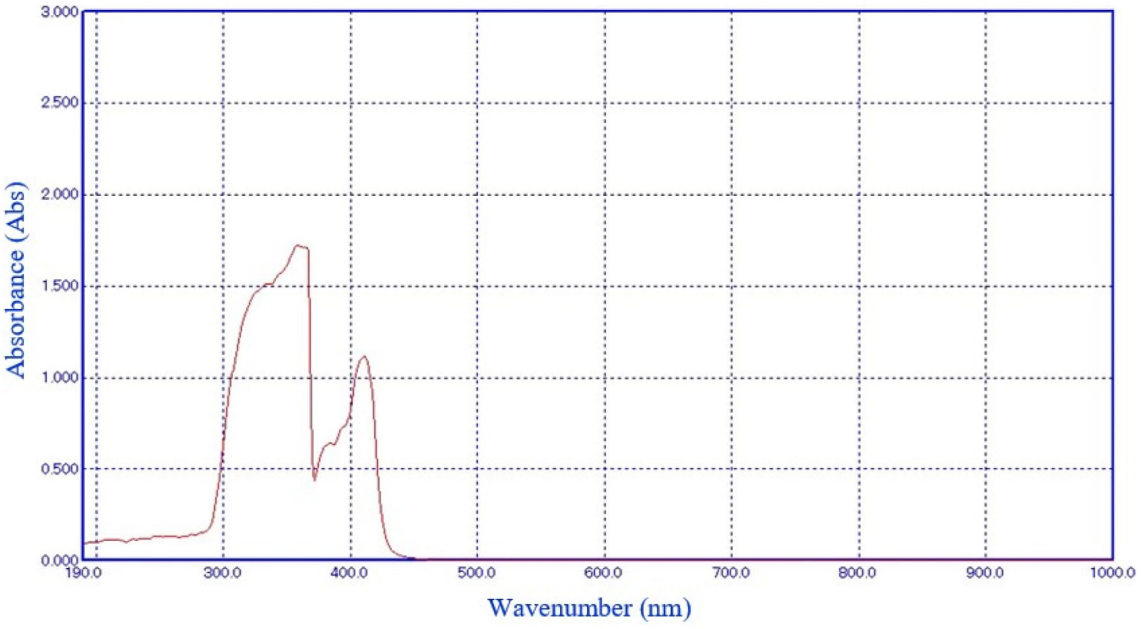

FIGURE 6 UV–visible absorption spectra of Anycubic eco UV resin

FFF. The uncured resins were reused after restoring the oxygen level to maintain the threshold intensity and successfully printed 3D objects. The Jaccard similarity coefficient 'J' generates a measure between 0 and 1 to access the target object (O_T) with the regenerated object (O_R). So, when the two objects coincide precisely, the Jaccard coefficient is one, which would be the ideal scenario. Any value above 0.9 is considered to be good. It is observed that Jaccard's similarity coefficient improves when the number of angular projections is increased. The Jaccard similarity coefficient is represented in Equation (3) and the reconstructed target object was similar to the actual one when the number of angular projections was 360.

$$J = \frac{|O_R \cap O_T|}{|O_R \cup O_T|} \tag{3}$$

The UV–Visible absorption spectrum of Anycubic Eco UV resin is plotted in Figure 6. The resin is sensitive

15482634, 0, Downloaded from https://onlinelibrary.wiley.com/doi/10.1002/pen.26186 by Egyptian National Sci. Network (Enstinet), Wiley Online Library on [09/11/2022]. See the Terms and Conditions (https://onlinelibrary.wiley.com/terms-and-conditions) on Wiley Online Library for rules of use; OA articles are governed by the applicable Creative Commons License

to lights having a wavelength from 355 nm to 410 nm. The wavelength was set to 405 nm as in many stereolithography 3D printers. The absorbance relations based on Beer–Lambert law are shown below:

$$A(\lambda) = -\log_{10} T(\lambda) \tag{4}$$

$$A(\lambda) = \epsilon(\lambda) \times c \times l \tag{5}$$

The resin absorptivity was calculated from the penetration depth and was obtained as 4.69×10^{-3} μm^{-1}. The response of Anycubic Eco UV resin with varying intensity and time of initiation of photopolymerization is calculated. A linear fit is plotted for the variation of onset of solidification time with respect to varying intensity values. The material response of the photopolymer resin is shown in Figure 7. The curing dosage required for the

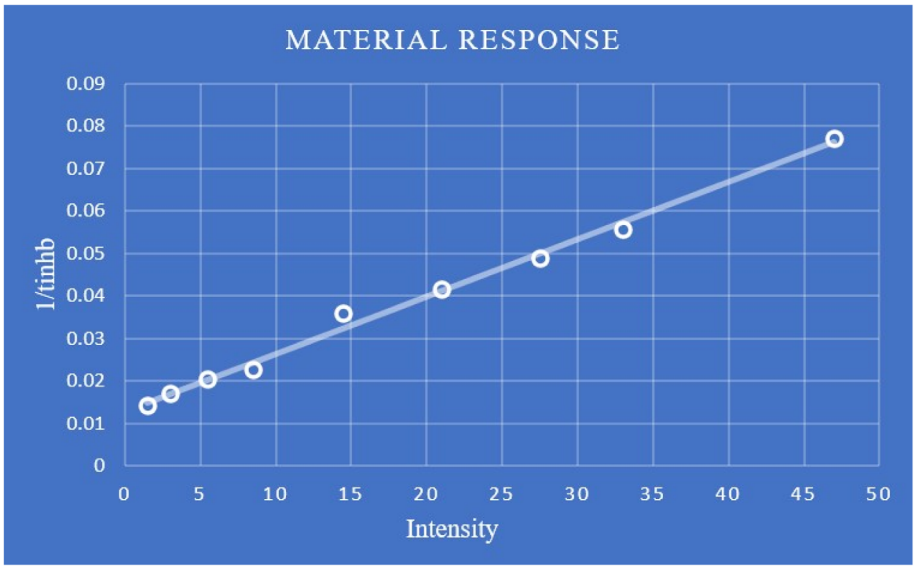

FIGURE 7 Material response of Anycubic eco UV resin

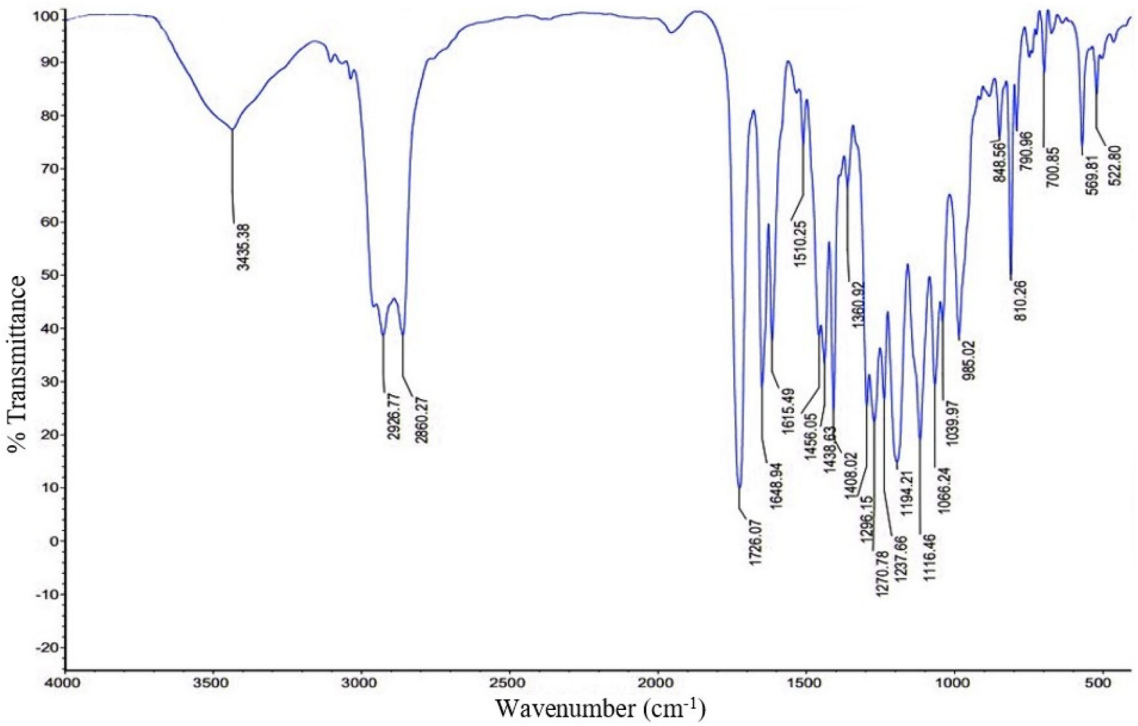

FIGURE 8 FTIR spectroscopy of Anycubic eco UV resin

15482634, 0, Downloaded from https://onlinelibrary.wiley.com/doi/10.1002/pen.26186 by Egyptian National Sci. Network (Enstinet), Wiley Online Library on [09/11/2022]. See the Terms and Conditions (https://onlinelibrary.wiley.com/terms-and-conditions) on Wiley Online Library for rules of use; OA articles are governed by the applicable Creative Commons License

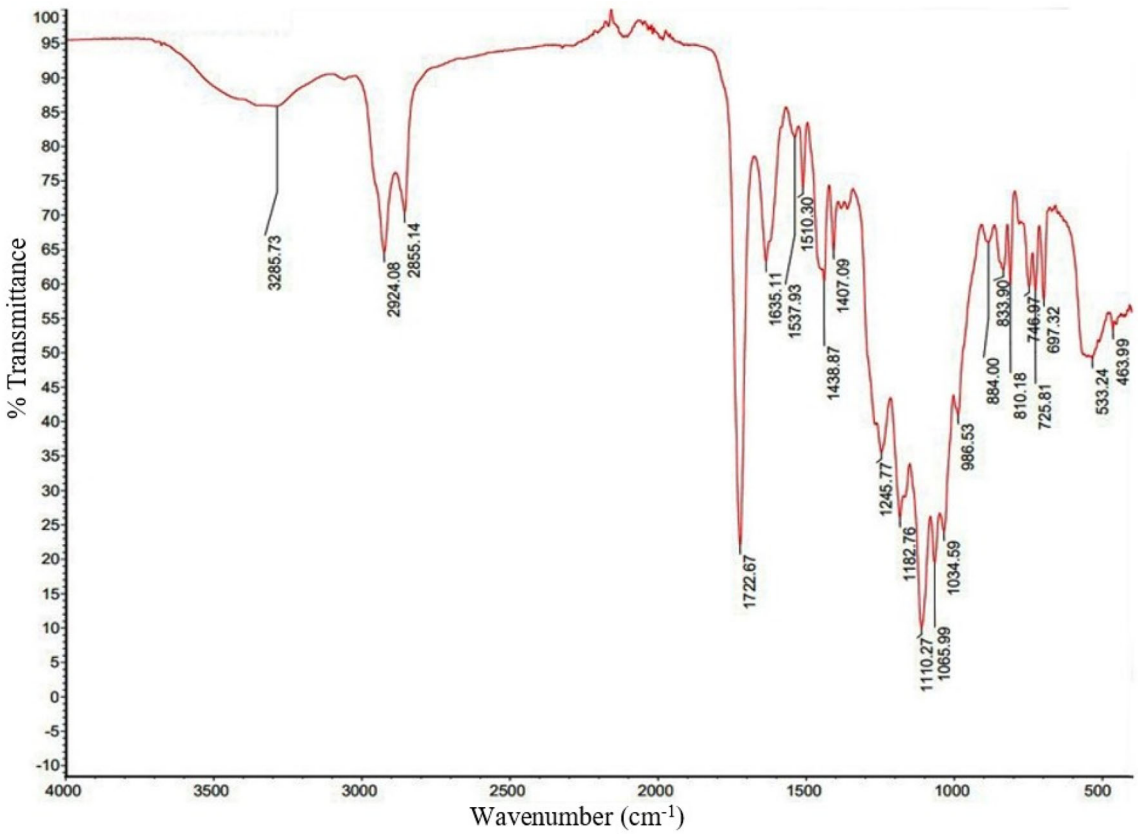

FIGURE 9 FTIR spectroscopy of cured Anycubic eco UV resin

TABLE 2 FTIR interpretation

Wavenumber	Appearance	Group	Compound
Functional groups			
3435	Medium, broad	N–H stretching	Aliphatic primary amine
2926, 2860	Medium	C–H stretching	Alkane
1726	Strong	C=O stretching	Aldehyde/α, β unsaturated ester
1648, 1615	Strong	C=C stretching	Alkene/α, β unsaturated ketone
1510	Strong	N–O stretching	Nitro compound
Fingerprint region			
1456, 1438, 1408	Strong	C–H bending	Alkane
1360	Medium	O–H bending	Alcohol
1296, 1270, 1237, 1194	Strong	C–O stretching	Aromatic ester/ alkyl aryl ether
1116, 1066, 1039	Strong	C–O stretching	Alcohol
985	Strong	C=C bending	Alkene
848	Medium	C–H bending	1, 4-disubstituted/ 1,2,3,4-tetrasubstituted
810	Strong	C=C bending	Alkene
790	Medium	C=C bending	Alkene
700			Benzene derivative
569, 522	Strong	C–I stretching	Halo compound

15482634, 0, Downloaded from https://onlinelibrary.wiley.com/doi/10.1002/pen.26186 by Egyptian National Sci. Network (Enstinet), Wiley Online Library on [09/11/2022]. See the Terms and Conditions (https://onlinelibrary.wiley.com/terms-and-conditions) on Wiley Online Library for rules of use; OA articles are governed by the applicable Creative Commons License

initiation of photopolymerization is calculated using Equation (6).[28]

$$D_C = \frac{\alpha e^{-\alpha R}}{SE_p} \tag{6}$$

The minimum time needed for curing is formulated next. Any point lying inside the container starts polymerizing at time T_c as the total absorption within a volume attains the curing dosage D_C. The photon flux can be represented based on the Beer–Lambert law as shown in Equation 7. The photon absorption rate is calculated using Equation (8).

$$\Phi = \Phi_0 e^{-\alpha z} \tag{7}$$

TABLE 3 Composition of Anycubic eco UV resin

Composition	Use	Percentage
Epoxidized soybean oil	Plasticizer	45%
Isooctyl acrylate	Acrylate monomer	30%
Ditrimethylolpropane tetraacrylate	Acrylate monomer	15%
2-hydroxy-1-[4-[[4-(2-hydroxy-2-methylpropanoyl)phenyl] methyl]phenyl]-2-methylpropan-1-one	Photoinitiator	5%
Polychloro copper phthalocyanine	Coloring pigment	5

$$B = -\frac{d\Phi}{dz} = \alpha\Phi_0 e^{-\alpha z} \tag{8}$$

The minimum time needed for the initiation of the curing process is T_C and the radius of the container is 'R'. The total energy received after 'T_C' would be equal to the required curing dosage and can be represented as:

$$D_C = \alpha\Phi_0 e^{-\alpha R} T_C \tag{9}$$

On rearranging,

$$T_c = \frac{D_C}{\alpha\Phi_0 e^{-\alpha z}} \tag{10}$$

where, $A(\lambda)$ is the absorbance at a specified wavelength λ, $T(\lambda)$ is the transmittance at a specified wavelength λ, $\epsilon(\lambda)$ is the molar absorption coefficient at a specified wavelength λ (m^{-1}), c is the molar concentration, l is the cuvette length (m), D_p is the penetration depth (m), α is the resin absorptivity (m^{-1}), R is the radius of the container (m), S is the slope of the $1/t_{inhb}$ versus intensity plot ($s^{-1}\ m^2\ W^{-1}$), t_{inhb} is the inhibition time (s), E_p is the energy of the 405 nm photon (J), Φ is the photon flux (photons $m^{-2}\ s^{-1}$), Φ_0 is the incident surface photon flux (photons $m^{-2}\ s^{-1}$), and B is the light absorption rate/volume (photons $m^{-3}\ s^{-1}$).

FTIR spectroscopy was done to analyze the bonding and functional groups of Anycubic Eco UV resin. Comparative studies between liquid and cured resins were also performed. Infrared radiation is delivered to a specimen in FTIR analysis, and the absorption through the sample, or in certain situations, the reflection of the

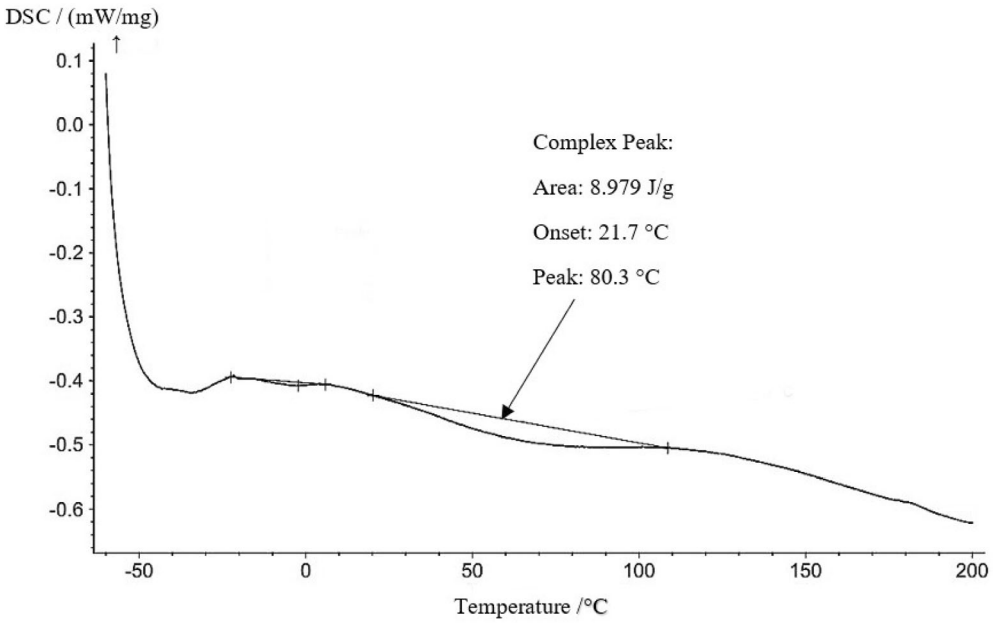

FIGURE 10 DSC curve of Anycubic eco UV resin

15482634, 0, Downloaded from https://onlinelibrary.wiley.com/doi/10.1002/pen.26186 by Egyptian National Sci. Network (Enstinet), Wiley Online Library on [09/11/2022]. See the Terms and Conditions (https://onlinelibrary.wiley.com/terms-and-conditions) on Wiley Online Library for rules of use; OA articles are governed by the applicable Creative Commons License

specimen, is evaluated as a function of frequency.[29] Covalent bonds among various elements consume light at several frequencies; hence, the absorption of infrared light at different bandwidths may be used to detect the molecular physicochemical characteristics of a substance. FTIR spectroscopy is a low-cost, quick method that requires less processing time. FTIR results for liquid and cured Anycubic Eco UV resin are shown in Figures 8 and 9, respectively. The chemical bonds of the resin are explained in Table 2. The larger percentage of C=O bonds represents better polymerization and degree of cure. Thereby, it enhances the stiffness and elastic modulus of the specimen. The two plots clearly show the difference in absorbance values in liquid and cured states. The absorbance level at different wavenumbers reduces in the cured solid part due to the conversion of bonds formed and cross-linking. The network creation results in the utilization of chemical bonds and hence lowers the absorbance levels. The absorption peaks at 3435, 1726, and 810 cm^{-1} correspond to the NH stretching, C=O stretching, and C=C bending of the urethane acrylate. The conversion of acrylic bonds during the cross-linking phenomenon is clear from the FTIR plots. The composition of the Anycubic Eco UV resin is shown in Table 3. The acrylate-based resin demonstrates a fast curing process due to the free radical photoinitiation process.

Figure 10 shows the DSC curve of Anycubic Eco UV resin. DSC enables a comprehensive analysis of melting and crystallization, which is critical for selecting materials and molding procedures.[30] The working temperature of the resin should be kept below 80°C during the curing process as the thermal deformation starts at around 80°C. The reaction enthalpy of the process is obtained as 8.979 J/g from the DSC curve plotted below. The starting temperature and end temperature of the reaction is 21.7°C and 80.3°C, respectively.

The fabrication of sample 3D objects and the over-printing illustration is explained in Figure 11. The rotation rate of the container should be within 1–5 rpm and the angular rotation should be 6°–30°/s. The surface roughness of the parts fabricated using VAM was obtained at the sub-micron level making it a precision manufacturing process. The R_a values were obtained in a range from 0.67 μm to 2.7 μm. The stair-casing effects found in the traditional layer-by-layer techniques were eliminated due to the volumetric photopolymerization. The relative error percentage of actual models and CAD models for different geometries is shown in Table 4. A maximum dimensional change of 5% was achieved using the in-house developed VAM printer. A cylinder of height and diameter of 1 cm each was fabricated to compare the processing speed of FFF, projection SLA, and VAM. FFF and SLA took 54 mins and 46 mins, respectively, with process parameters selected for highest quality whereas VAM was fabricated in less than a minute. Post-processing time was not calculated for the above. Minimum post-curing should be provided for complete cross-linking and thereby enhancement in the mechanical properties could be easily achieved. The curing box having 40 W intensity could be employed for delivering the necessary UV light for the entire cross-

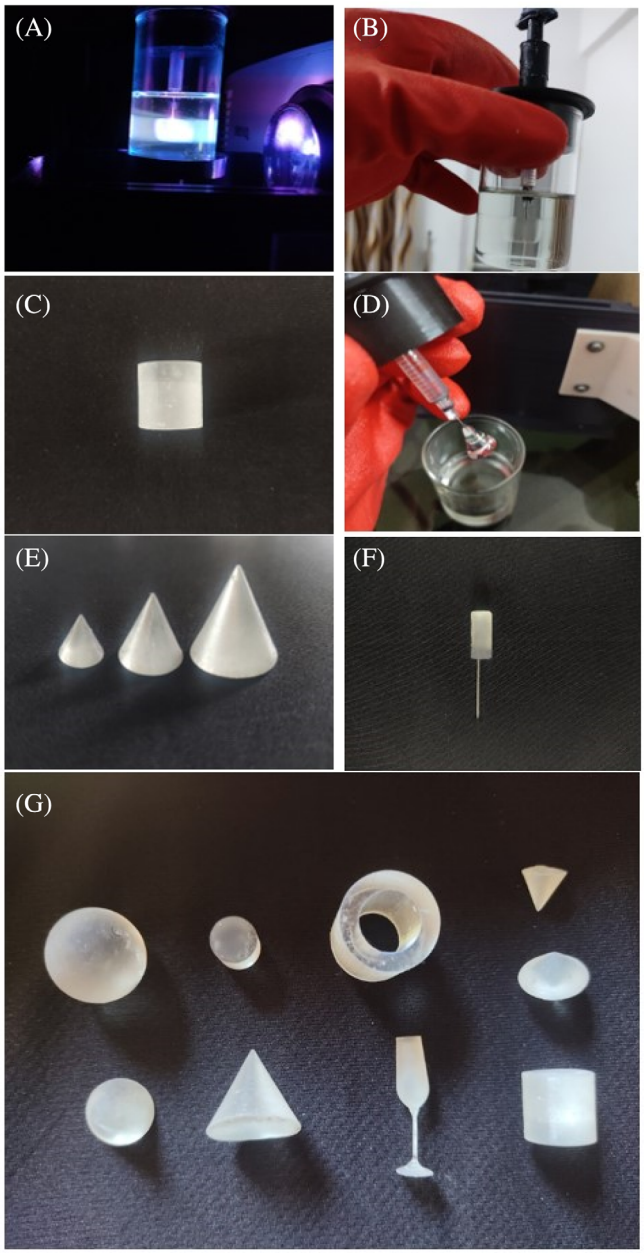

FIGURE 11 (A) Curing of the cylinder specimen, (B) cylinder formed inside the resin container, (C) cylinder of 1 cm height and diameter fabricated, (D) cone of 1 cm diameter and 1.5 cm height being lifted, (E) cones having three different diameters and height fabricated, (F) illustration of over-printing, and (G) different shapes printed using VAM

15482634, 0, Downloaded from https://onlinelibrary.wiley.com/doi/10.1002/pen.26186 by Egyptian National Sci. Network (Enstinet), Wiley Online Library on [09/11/2022]. See the Terms and Conditions (https://onlinelibrary.wiley.com/terms-and-conditions) on Wiley Online Library for rules of use; OA articles are governed by the applicable Creative Commons License

TABLE 4 Dimensional deviations

Geometry	Dimension	CAD model (mm)	Printed specimen (mm)	Relative error (%)
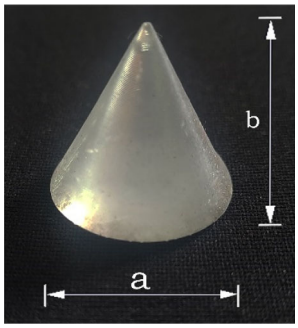	a	10	9.88	−1.2
	b	15	15.72	4.8
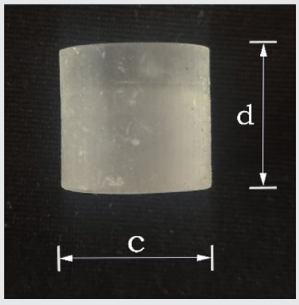	c	10	9.92	−0.8
	d	10	10.35	3.5
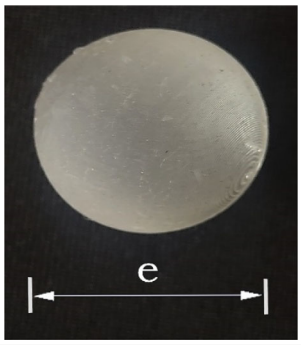	e	20	19.47	−2.65

TABLE 5 Compressive strength at various curing times

Curing time (min)	Compressive strength (MPa)
15	25.56
30	30.29
45	33.89
60	33.65

linking. A maximum part size of 8 cm^3 was fabricated inside the 50 ml Borosil container using the VAM printer having the SVGA resolution DLP projector.

Post-curing analysis was performed on the ASTM D695 components volumetrically fabricated using the developed printer. The UV curing box was employed to perform the post-processing investigations. The cylindrical testing samples had a diameter of 12.7 mm and a height of 25.4 mm, respectively. The samples were placed in the curing box with 40 W UV lighting for a time period of 15, 30, 45, and 60 minutes. Compressive strength testing was conducted on Shimadzu AG-X plus 10 kN UTM machine and an average of three samples were taken for each post-processing condition. The compressive strength of Anycubic Eco UV resin cylindrical components was found to be 13.52 MPa without any post-curing treatment. The compression strength was recorded at a maximum strain percentage of 5%. Post-curing of 45 minutes duration produced an enhancement of approximately 150%. Optimized UV curing time was obtained as 45 minutes. The compressive strength values of ASTM D695 Anycubic Eco UV resin cylindrical components at various curing time are shown in Table 5. The UV curing helped in the cross-linking of uncured regions and thereby resulted in improved mechanical properties. Maximum compressive strength of 33.89 MPa has achieved after 45 minutes of UV curing and a further increase in curing time did not show any increase in strength values.

15482634, 0, Downloaded from https://onlinelibrary.wiley.com/doi/10.1002/pen.26186 by Egyptian National Sci. Network (Enstinet), Wiley Online Library on [09/11/2022]. See the Terms and Conditions (https://onlinelibrary.wiley.com/terms-and-conditions) on Wiley Online Library for rules of use; OA articles are governed by the applicable Creative Commons License

4 | CONCLUSIONS

The development of a low-cost volumetric 3D printer using commercially available less viscous Anycubic plant-based environment-friendly resin is demonstrated in this study. Centimeter scale objects could be manufactured in as low as 30 s time. Apart from traditional 3D printing methodologies employing repetitive unit operations to fabricate complex geometries, VAM technology cures the entire 3D specimen within the rotating container. Thereby, the major limitations such as low surface quality and mechanical strength could be easily overcome. Dimensional deviations of less than 5% from the actual CAD data could be achieved with this in-house fabricated volumetric printer. An outer container having resin without photo-initiators could be used to avoid the refraction level while fabricating. Different optimization approaches for projections, larger scaling of volumetric printing, material diversity, etc., could be the possible future scope of the fastest 3D printing technology reported so far.

ACKNOWLEDGMENTS

The authors would like to acknowledge the Principal and Head of Mechanical Engineering Department, Government College of Engineering Kannur for the facilities provided to carry out research. The authors would like to thank TEQIP Four Funds, Government College of Engineering Kannur for funding this work. The authors would like to thank Dr. Mythreyi Unni, Research Scientist at Core Quantum Technologies, Inc., United States for the technical support in chemical characterization. The authors wish to thank Mr. Mathew Varghese Anamala for the support provided during the experimentation.

CONFLICT OF INTEREST

The authors declare that they have no known competing financial interests or personal relationships that could have appeared to influence the work reported in this paper.

OWNERSHIP

The authors declare that the submitted work is our own and that copyright has not been breached in seeking its publication.

ORIGINALITY

The authors declare that the submitted work has not previously been published in full and is not being considered for publication elsewhere.

DATA AVAILABILITY STATEMENT

The data that support the findings of this study are available from the corresponding author upon reasonable request.

ORCID

Ribin Varghese Pazhamannil https://orcid.org/0000-0001-9725-6640

REFERENCES

[1] L. Chen, Y. He, Y. Yang, S. Niu, H. Ren, *Int. J. Adv. Manuf. Technol.* **2017**, *89*(9), 3651.
[2] T. A. Salet, Z. Y. Ahmed, F. P. Bos, H. L. Laagland, *Virtual Phys. Prototyp.* **2018**, *13*(3), 222.
[3] X. Han, Y. Zhang, J. Tian, T. Wu, Z. Li, F. Xing, S. Fu, *Polym. Eng. Sci.* **2022**, *62*(1), 3.
[4] I. Bahnini, M. Rivette, A. Rechia, A. Siadat, A. Elmesbahi, *Int. J. Adv. Manuf. Technol.* **2018**, *97*(1), 147.
[5] N. Shahrubudin, T. C. Lee, R. Ramlan, *Procedia Manuf.* **2019**, *35*, 1286.
[6] C. C. Seepersad, *Addit. Manuf.* **2014**, *1*(1), 10.
[7] R. V. Pazhamannil, N. V. N. Jishnu, P. Govindan, A. Edacherian, *Polym. Eng. Sci.* **2022**, *62*(5), 1356.
[8] H. Long, Z. Wu, Q. Dong, Y. Shen, W. Zhou, Y. Luo, C. Zhang, X. Dong, *Polym. Eng. Sci.* **2019**, *59*(2), 247.
[9] H. L. Van Der Laan, M. A. Burns, T. F. Scott, *ACS Macro Lett.* **2019**, *8*(8), 899.
[10] B. Huang, R. Hu, Z. Xue, J. Zhao, Q. Li, T. Xia, W. Zhang, C. Lu, *Carbohydr. Polym.* **2020**, *231*, 115736.
[11] M. Regehly, Y. Garmshausen, M. Reuter, N. F. König, E. Israel, D. P. Kelly, C. Y. Chou, K. Koch, B. Asfari, S. Hecht, *Nature* **2020**, *588*(7839), 620.
[12] J. R. Tumbleston, D. Shirvanyants, N. Ermoshkin, R. Janusziewicz, A. R. Johnson, D. Kelly, K. Chen, R. Pinschmidt, J. P. Rolland, A. Ermoshkin, E. T. Samulski, *Science* **2015**, *347*(6228), 1349.
[13] C. L. Caudill, J. L. Perry, S. Tian, J. C. Luft, J. M. DeSimone, *J. Controlled Release* **2018**, *284*, 122.
[14] M. Ali, A. Nazir, J. Y. Jeng, *Int. J. Adv. Manuf. Technol.* **2020**, *111*(11), 3273.
[15] M. Shusteff, A. E. Browar, B. E. Kelly, J. Henriksson, T. H. Weisgraber, R. M. Panas, N. X. Fang, C. M. Spadaccini, *Sci. Adv.* **2017**, *3*(12), 5496.
[16] C. M. Rackson, K. M. Champley, J. T. Toombs, E. J. Fong, V. Bansal, H. K. Taylor, M. Shusteff, R. R. McLeod, *Addit. Manuf.* **2021**, *48*, 102367.
[17] D. Loterie, P. Delrot, C. Moser, *Nat. Commun.* **2020**, *11*(1), 1 852.
[18] C. C. Cook, E. J. Fong, J. J. Schwartz, D. H. Porcincula, A. C. Kaczmarek, J. S. Oakdale, B. D. Moran, K. M. Champley, C. M. Rackson, A. Muralidharan, R. R. McLeod, *Adv. Mater.* **2020**, *32*(47), 2003376.
[19] J. J. Schwartz, D. H. Porcincula, C. C. Cook, E. J. Fong, M. Shusteff, *Polym. Chem.* **2022**, *13*(13), 1813.
[20] J. T. Toombs, M. Luitz, C. C. Cook, S. Jenne, C. C. Li, B. E. Rapp, F. Kotz-Helmer, H. K. Taylor, *Science* **2022**, *376*(6590), 308.
[21] M. Kollep, G. Konstantinou, J. Madrid-Wolff, A. Boniface, L. Hagelüken, P. V. Sasikumar, G. Blugan, P. Delrot, D. Loterie, J. Brugger, C. Moser, *Adv. Eng. Mater.* **2022**, *24*, 2101345.
[22] C. M. Rackson, J. T. Toombs, M. P. De Beer, C. C. Cook, M. Shusteff, H. K. Taylor, R. R. McLeod, *Opt. Lett.* **2022**, *47*(5), 1279.
[23] I. Bhattacharya, J. Toombs, H. Taylor, *Addit. Manuf.* **2021**, *47*, 102299.

15482634, 0, Downloaded from https://onlinelibrary.wiley.com/doi/10.1002/pen.26186 by Egyptian National Sci. Network (Enstinet), Wiley Online Library on [09/11/2022]. See the Terms and Conditions (https://onlinelibrary.wiley.com/terms-and-conditions) on Wiley Online Library for rules of use; OA articles are governed by the applicable Creative Commons License

[24] J. Madrid-Wolff, A. Boniface, D. Loterie, P. Delrot, C. Moser, *Adv. Sci.* **2022**, *9*(22), 2105144. https://doi.org/10.1002/advs.202105144.

[25] A. V. Salvekar, F. H. Nasir, Y. H. Chen, S. Maiti, V. D. Ranjan, H. M. Chen, H. Wang, W. M. Huang, *3D Print. Addit. Manuf.* **2022**. https://doi.org/10.1089/3dp.2021.0279

[26] A. Orth, K. L. Sampson, Y. Zhang, K. Ting, D. A. van Egmond, K. Laqua, T. Lacelle, D. Webber, D. Fatehi, J. Boisvert, C. Paquet, *Addit. Manuf.* **2022**, *56*, 102869. https://doi.org/10.1016/j.addma.2022.102869.

[27] J. Madrid-Wolff, G. Konstantinou, D. Loterie, P. Delrot, C. Moser, *The European Conference on Lasers and Electro-Optics*, Optica Publishing Group, Washington, DC **2021**.

[28] B. E. Kelly, I. Bhattacharya, H. Heidari, M. Shusteff, C. M. Spadaccini, H. K. Taylor, *Science* **2019**, *363*(6431), 1075.

[29] A. Barkane, O. Platnieks, M. Jurinovs, S. Gaidukovs, *Polym. Degrad. Stab.* **2020**, *181*, 109347.

[30] K. Sawicz-Kryniger, P. Niezgoda, P. Stalmach, K. Starzak, A. Wysocka, T. Swiergosz, R. Popielarz, *Eur. Polym. J.* **2022**, *162*, 110933.

How to cite this article: R. V. Pazhamannil, H. M. Hadidi, G. Puthumana, *Polym. Eng. Sci.* **2022**, 1. https://doi.org/10.1002/pen.26186

15482634, 0, Downloaded from https://onlinelibrary.wiley.com/doi/10.1002/pen.26186 by Egyptian National Sci. Network (Enstinet), Wiley Online Library on [09/11/2022]. See the Terms and Conditions (https://onlinelibrary.wiley.com/terms-and-conditions) on Wiley Online Library for rules of use; OA articles are governed by the applicable Creative Commons License